Journal of CO2 Utilization 67 (2023) 102343

Contents lists available at ScienceDirect

Journal of CO2 Utilization

journal homepage: www.elsevier.com/locate/jcou

How the presence of O_2 and NO_x influences the alternate cycles of CO_2 adsorption and hydrogenation to CH_4 on Ru-Na-Ca/Al_2O_3 dual function material

Alejandro Bermejo-López, Beñat Pereda-Ayo, Jon A. Onrubia-Calvo, José A. González-Marcos, Juan R. González-Velasco *

Department of Chemical Engineering, Faculty of Science and Technology, Universidad del País Vasco UPV/EHU, Barrio Sarriena, s/n, 48940 Leioa, Bizkaia, Spain

ARTICLE INFO

Keywords:
CO_2 hydrogenation
Integrated CO_2 capture and utilization
Methanation
Dual function material
Oxidant species
O_2 and NO_x effect

ABSTRACT

The Integrated Carbon Capture and Utilization-Methanation (ICCU-Methanation) requires a Dual Function Material (DFM), which firsts captures CO_2 and then converts it into CH_4, working in alternating adsorption and hydrogenation periods. The ICCU technology can be applied directly to a flue gas leaving a combustion chamber, which usually contains oxidizing species such as oxygen and nitrogen oxides. In this work, the stability of a DFM with composition 4%Ru-8%Na_2CO_3-8%CaO/Al_2O_3 is studied for the CO_2 adsorption and hydrogenation in alternate cycles including O_2 (0–10%) and NO_x (0–2000 ppm) during the adsorption period. The variation of CO_2 concentration in the usual range of flue gases (5–15%) has little influence on the global performance of the ICCU technology. However, the incorporation of O_2 during the adsorption period decreases the production of CH_4, and this decrease is even accentuated with increasing the oxygen concentration. This fact is mainly attributed to the oxidation of metal sites that limits the reduction behavior. On the other hand, the addition of NO_x competes with CO_2 for the basic adsorption sites, which slightly limits the amount of CO_2 stored, and consequently the production of CH_4. Helpfully, the proposed DFM presents high stability during the 207 cycles here performed, which corresponds to 34 h of time-on-stream, including different CO_2 concentrations, and in the presence or absence of O_2 and/or NO_x. It is concluded that the proposed DFM formulation is competent for long-term operation in the presence of O_2 and NO_x during the CO_2 adsorption period.

1. Introduction

The Intergovernmental Panel on Climate Change (IPCC) stresses the importance of reaching net zero CO_2 emissions by 2050, while a dramatic decrease must occur after 2030 if it is expected to limit the global temperature increase below 1.5 °C [1]. As CO_2 emissions increase due to fossil fuels, it is imperative that the energy system focus on renewable energy sources [1,2]. However, increasing renewable energy production solely will not be enough to meet this target. At this point, CO_2 capture should also play an important role for the decarbonization of industrial sectors [3]. Once CO_2 is captured, it must either be stored (carbon capture and storage, CCS) or utilized (carbon capture and utilization, CCU) [4–7]. CCS is highly energy consumer; however, the conversion into fuels and chemical products stands out as a more promising alternative. In fact, with CCU the recycling of CO_2 would be achieved, thus closing the carbon cycle [1,8].

Recently, to avoid energy penalties associated with the regeneration and compression steps required for CO_2 transportation, researchers have attempted to integrate CO_2 capture and utilization in a single process [9], which is called Integrated Carbon Capture and Utilization, ICCU [10]. An even renewed interest for such procedure was observed after the increase of oil price in the early 2010's and has been reinforced with the growing awareness of the impact of CO_2 as a greenhouse gas [1,3, 11–14]. In this strategy, the captured CO_2 is transformed in the same place into value-added products.

The ICCU technology is carried out using Dual Function Materials (DFM). The operation is performed alternating adsorption and regeneration periods in which the feed streams are modified. This novel operating strategy was proposed for the first time in 2015 by the Farrauto's group for the capture of CO_2 and hydrogenation to CH_4 [15]. Beyond methanation, DFMs have also been developed for the reverse water gas shift reaction (RWGS), dry reforming of methane (DRM), and

* Corresponding author.
E-mail address: juanra.gonzalezvelasco@ehu.eus (J.R. González-Velasco).

https://doi.org/10.1016/j.jcou.2022.102343
Received 22 August 2022; Received in revised form 4 November 2022; Accepted 24 November 2022
Available online 29 November 2022

dry ethane reforming (DER) [12]. However, the process of capture and conversion to CH_4 is the most promising and therefore the most studied [1].

The DFMs for methanation are composed of an adsorbent material to capture CO_2 and a catalytic metal for hydrogenation. Both phases are supported on a high surface carrier, being γ-Al_2O_3 the most widely used as achieving the best results [16]. The adsorbent phases are commonly based on Ca, Na, Ba, Mg or K [17–25]. On the other hand, Ru, Ni and Rh are used as catalytic metals [17–25]. In own previous work [26], the simultaneous presence of Na and Ca in the same Ru-DFM has been studied, where the sample basicity was modulated by varying the Na_2CO_3/CaO ratio, which allowed improving the CH_4 production. The DFM 4%Ru-8%Na_2CO_3-8%CaO/γ-Al_2O_3 has been selected there as the optimal formulation.

Flue gases have usually a CO_2 concentration between 5% and 15%, depending on the fuel used and the characteristics of the combustion process. In addition, flue gases also present notable concentration of O_2 and H_2O, as well as lower concentrations of NO_x and SO_x [1]. Several studies have been published on the influence of realistic flue gas conditions on the CO_2 adsorption and hydrogenation performance [16,24,27–32]. Nickel-based DFMs are used because of good relationship between activity and price. The price, per unit mass, compared to Ru, is about 2000 times lower. In the absence of O_2 in the flue gas, like in e.g. brewery exhausts, Ni could potentially become the best alternative. Nevertheless, the presence of oxygen during the adsorption period significantly limits the activity of Ni [16]. As the flue gas streams usually contain O_2, Ru-Based DFMs are the ideal candidate in realistic flue gas conditions because the reduction of RuO_x to its metallic state (active for methanation) is easier compared to other metals, such as Ni [1,31].

The presence of O_2 and H_2O has been studied in several publications [16,24,27–32]; however, the presence of NO_x has only recently been studied by Porta et al. [30]. These authors carried out cycles feeding 1% CO_2, 2.5% H_2O, 3% O_2 and 500 ppm of NO_x during the adsorption period. They observed a competitive adsorption between CO_2 and NO_x. With the inclusion of H_2 in the hydrogenation period, they did not detect the formation of C-containing species, either CH_4 or CO.

In this work, the influence of the inclusion of oxidizing species, such as O_2 and NO_x, on the CO_2 adsorption and hydrogenation performance of a DFM is assessed. Oxygen can partially oxidize the metallic phase, leading to some activity loss. NO_x is also a powerful oxidant (higher than O_2), which can also affect the redox properties of the metallic phase. Besides, the acidic nature of NO_x suggests a competition with CO_2 for the basic storage sites of the DFM. The previously optimized DFM 4%Ru-8% Na_2CO_3-8%CaO/γ-Al_2O_3 has been selected for the study. The viability of this DFM for long-term operation including oxidant species during the CO_2 adsorption period is also studied. For that, the influence of CO_2 concentration in the range 1.5–15% is analysed. On the other hand, the influence of the presence of different concentrations of O_2 (1–10%) and NO_x (400–2000 ppm), during the adsorption period is studied separately. In the same way, the joint presence of O_2 and NO_x is also analysed. Finally, the influence of the long-term operation (in the presence of O_2 and NO_x) on the physicochemical properties of DFM is analysed.

2. Experimental

2.1. DFM preparation

The DFM 4%Ru-8%Na_2CO_3-8%CaO/γ-Al_2O_3 was prepared by wetness impregnation. First, appropriated amounts of $Ca(NO_3)_2{\cdot}4H_2O$ (*Merck*) and Na_2CO_3 (*Riedel de-Haën*) were impregnated over γ-Al_2O_3 (*Saint Gobain*). The impregnated powder was dried at 120 °C overnight and then calcined at 400 °C for 4 h (1 °C min^{-1}). Afterwards, Ru(NO) $(NO_3)_2$ (*Sigma Aldrich*) was impregnated over the previous calcined powder. After drying at 120 °C, the sample was stabilized by calcination at 400 °C for 4 h (1 °C min^{-1}). The nominal loadings of Na_2CO_3 and CaO were 8% wt. each, and 4% wt. for ruthenium.

2.2. Reactor testing

The catalytic activity in alternate cycles of CO_2 adsorption and hydrogenation to CH_4 for the DFM 4%Ru-8%Na_2CO_3-8%CaO/γ-Al_2O_3 was evaluated in a vertical tubular stainless steel reactor. The reactor was loaded with 1 g of DFM whose particle size was between 0.3 and 0.5 mm. Prior to the cycles, the DFM was reduced (once every day) with a stream composed of 10% H_2/Ar. First, the temperature was increased from RT to 400 °C and then was maintained for 60 min. Once this reduction pretreatment was completed, the temperature was stabilized at 340 °C in Ar and alternated cycles of CO_2 adsorption and hydrogenation to CH_4 started. During the adsorption period, a stream composed of X% CO_2, Y % O_2 and Z ppm of NO (X, Y and Z as specified in Table 1, and Ar balance) was fed for 1 min, followed by a purge with Ar for 2 min to remove weakly adsorbed CO_2. The number of cycle, the day that the experiment was done and the temperature are also summarized in the Table 1. Next, during the hydrogenation period, a stream consisting of 10% H_2/Ar was fed for 2 min, followed by an Ar purge for 1 min before starting the adsorption period again. The composition of the gas stream admitted to the reactor during the hydrogenation period was the same for the 207 cycles carried out. The total flow rate in both periods was 1200 cm^3 min^{-1}, which corresponds to a space velocity of 45,000 h^{-1}. The flue gas composition was continuously monitored using the *MultiGas 2030 FT-IR* analyzer for quantitative analysis of CO_2, CH_4, CO, H_2O, NO, NO_2, NH_3

Table 1
Detailed compositions of the different streams for the adsorption period together with the number of cycle, the day that the experiment was done and the temperature.

Cycle number	Day	Adsorption period feed	T, °C
hyd. 60 min	1	–	400
1–7	1	1.5% CO_2	340
8–12	1	5% CO_2	340
13–17	1	10% CO_2	340
18–22	1	15% CO_2	340
23–29	1	1.5% CO_2	340
30–34	1	1.5% CO_2 + 10% O_2	340
35–44	1	10CO_2	340
hyd. 60 min	2	–	400
45–54	2	10% CO_2	340
55–59	2	10% CO_2 + 1% O_2	340
60–64	2	10% CO_2 + 5% O_2	340
65–69	2	10% CO_2 + 10% O_2	340
70–79	2	10% CO_2	340
80–84	2	10% CO_2 + 10% O_2	340
85–89	2	10% CO_2	340
90–94	2	10% CO_2 + 10% O_2	340
hyd. 28 min	2	–	340
95–99	2	10% CO_2	340
100–104	2	10% CO_2 + 10% O_2	340
hyd. 60 min	3	–	400
105–111	3	1.5% CO_2	340
112–116	3	1.5% CO_2 + 400 ppm NO	340
117–121	3	10% CO_2	340
122–126	3	10% CO_2 + 400 ppm NO	340
127–132	3	10% CO_2 + 800 ppm NO	340
132–136	3	10% CO_2 + 1200 ppm NO	340
137–142	3	10% CO_2 + 1600 ppm NO	340
142–146	3	10% CO_2 + 2000 ppm NO	340
147–152	3	1% CO_2	340
153–156	3	1.5% CO_2 + 2000 ppm NO	340
hyd. 60 min	4	–	400
157–166	4	10% CO_2	340
167–171	4	10% CO_2 + 400 ppm NO	340
172–176	4	10% CO_2 + 10% O_2 + 400 ppm NO	340
177–181	4	10% CO_2	340
182–186	4	10% CO_2 + 400 ppm NO	340
187–191	4	10% CO_2 + 10% O_2 + 400 ppm NO	340
hyd. 28 min	2	–	340
192–196	4	10% CO_2	340
197–201	4	10% CO_2 + 400 ppm NO	340
202–207	4	10% CO_2 + 10% O_2 + 400 ppm NO	340

and N_2O. The N_2 formation was qualitatively followed by mass spectrometry (*OMNI StarTM*) measuring the m/e= 28 signal. Additionally, between cycles 94–95 and 191–192 an additional hydrogenation was carried out with 10% H_2/Ar at 340 °C for 28 min. For that, the hydrogenation period of cycles 94 and 191 was prolonged up to 30 min

The CH_4, H_2O and CO productions were calculated from the following expressions:

$$Y_{CH_4}\left(\mu mol\ g^{-1}\right) = \frac{1}{W}\int_0^t F^{out}_{CH_4}(t)dt \quad (1)$$

$$Y_{H_2O}\left(\mu mol\ g^{-1}\right) = \frac{1}{W}\int_0^t F^{out}_{H_2O}(t)dt \quad (2)$$

$$Y_{CO}\left(\mu mol\ g^{-1}\right) = \frac{1}{W}\int_0^t F^{out}_{CO}(t)dt \quad (3)$$

The amount of CO_2 stored was calculated from Eq. (4). For that, the molar flux of CO_2 that leaves the reactor ($F^{out}_{CO_2}$) was subtracted from the molar flux fed ($F^{in}_{CO_2}$) and integrated along the duration of the storage period. To determine the molar flux of CO_2 fed, the stream from the feed system was led directly to the analyser (bypassing the reactor). This profile corresponds to the actual CO_2 input that was fed to the reactor. Besides, the amount of CO (Y_{CO}) and CH_4 (Y_{CH4}) produced during the adsorption period has to be subtracted in order to calculate the amount of CO_2 stored.

$$\text{stored } CO_2\left(\mu mol\ g^{-1}\right) = \frac{1}{W}\int_0^t \left[F^{in}_{CO_2}(t) - F^{out}_{CO_2}(t)\right] dt - Y_{CO}|_{ads} - Y_{CH_4}|_{ads} \quad (4)$$

CH_4 selectivity is determined by relating the CH_4 and CO productions since they were the only carbon based products that were detected:

$$S_{CH4}(\%) = \frac{Y_{CH_4}}{Y_{CH_4} + Y_{CO}} \times 100 \quad (5)$$

The carbon balance was checked with the following expression:

$$s_{CB}(\%) = \left(\frac{Y_{CH_4} + Y_{CO}}{stored\ CO_2} - 1\right) \times 100 \quad (6)$$

In the operation with NO_x, the amount of N-containing species was calculated by integrating the molar flux of the corresponding compound at the reactor outlet:

$$Y_{NO_x}\left(\mu mol\ g^{-1}\right) = \frac{1}{W}\int_0^t F^{out}_{NO_x}(t)dt \quad (7)$$

$$Y_{NH_3}\left(\mu mol\ g^{-1}\right) = \frac{1}{W}\int_0^t F^{out}_{NH_3}(t)dt \quad (8)$$

$$Y_{N_2O}\left(\mu mol\ g^{-1}\right) = \frac{1}{W}\int_0^t F^{out}_{N_2O}(t)dt \quad (9)$$

The amount of N_2 produced was calculated from the nitrogen by balance as follows:

$$Y_{N_2}\left(\mu mol\ g^{-1}\right) = \frac{Y^{in}_{NO_x} - Y^{out}_{NO_x} - Y^{out}_{NH_3} - 2Y^{out}_{N_2O}}{2} \quad (10)$$

Finally, the amount of NO_x stored was calculated by the following expression:

$$\text{stored } NO_x\left(\mu mol\ g^{-1}\right) = \frac{1}{W}\int_0^t \left[F^{in}_{NO_x}(t) - F^{out}_{NO_x}(t)\right] dt - Y_{NH_3}|_{ads} - 2Y_{N_2O}|_{ads} - 2Y_{N_2}|_{ads} \quad (11)$$

2.3. Characterization techniques

The specific surface area, pore diameter and pore volume were determined from the N_2 adsorption-desorption isotherms. The DFM before and after the activity test was pre-purged with nitrogen for 10 h at 300 °C using *SmartPrep degas system* (*Micromeritics*). Then, the analysis were carried out at the nitrogen boiling temperature (−196 °C) using an automated gas adsorption analyser (*TriStar II, Micromeritics*).

X-ray diffraction spectra were obtained in a *Philips PW1710* diffractometer. The DFM before and after the activity test were finely ground and were subjected to Cu Kα radiation in a continuous scan mode from 5° to 70° 2θ with 0.02 per second sampling interval.

Ruthenium dispersion before and after the activity test was determined using the H_2 chemisorption method in a *Micromeritics ASAP 2020* equipment. Prior to the experiments, the DFMs (0.2 g) were reduced with pure H_2 for 2 h at 400 °C. After that, the DFMs were degassed at the same temperature for 90 min. Finally, H_2 was dossed for obtaining the adsorption isotherm at 35 °C. Adsorption stoichiometry of Ru/H= 1 was assumed [33].

The morphology of the DFM before and after the activity test was analysed by transmission electron microscopy (TEM) in a *JEM-1400 Plus* instrument using a voltage of 100 kV. The reduced DFMs were dispersed in distillated water ultrasonically, and the solutions were then dropped on copper grids coated with lacey carbon film.

3. Results and discussion

As an overview of the study, Fig. S1 shows the evolution of CH_4 and CO productions for the 207 alternate cycles of CO_2 adsorption and hydrogenation to CH_4. The composition of the feed stream admitted to the reactor during the adsorption period is included in the figure for each cycle in accordance to the information detailed in Table 1. For a deeper understanding and a detailed discussion of the influence of gas stream composition on the overall CO_2 adsorption and hydrogenation performance, the results section is divided into different subsections. First, the global dynamics of the CO_2 adsorption and hydrogenation is briefly discussed, providing the basics for a better understanding of the following sections. Then, the influence of the CO_2 concentration is addressed (Fig. S1a). Next, the influence of the presence and concentration of O_2 (Fig. S1b) and NO (Fig. S1c) is studied separately. Finally, the influence of the joint presence of O_2 and NO (Fig. S1d) on the overall performance of the DFM is analyzed.

3.1. Global dynamics of the CO_2 adsorption and hydrogenation to CH_4

The first seven adsorption and hydrogenation cycles (Fig. S1a) are carried out by feeding a gas stream composed of 1.5% CO_2/Ar during adsorption period (1 min). Subsequently, the DFM is purged with Ar for 2 min. Finally, the hydrogenation period is carried out with a gas stream composed of 10% H_2/Ar for 2 min and another purge with Ar for 1 min to end the cycle and start the next one. Therefore, the total duration of each cycle containing adsorption, purge, hydrogenation and purge, is 6 min.

Fig. 1 shows the concentration profiles of CO_2, H_2O, CH_4 and CO with time at the outlet of the reactor for the seven consecutive cycles of CO_2 adsorption and hydrogenation to CH_4. The cycles (containing adsorption and hydrogenation periods and purges in between) are delimited by dashed lines for a better interpretation. In each cycle, a CO_2 peak is observed during the adsorption period, a CH_4 peak during the hydrogenation period and two H_2O peaks, one in each period. A very small production of CO is also detected in both periods. Note that the ordinate axis scale is 130 times smaller (ppm vs. %).

On the other hand, comparing the cycles with each other, except for the first ones, it can be seen that they tend to be identical. Therefore, it is confirmed that once the cycle-to-cycle steady state is reached, the process is cyclic and repetitive when only CO_2 is fed. The detailed

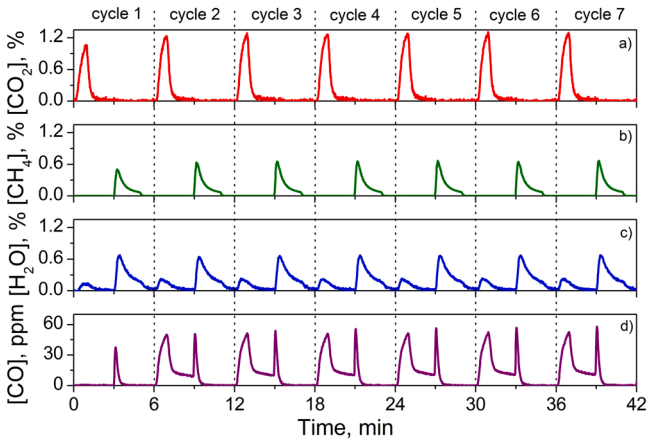

Fig. 1. CO_2, CH_4, H_2O and CO concentration profiles during the first seven cycles of CO_2 adsorption and hydrogenation to CH_4 with 1.5% CO_2 in the adsorption period.

Table 2
Proposed reactions in each period during cyclic of CO_2 adsorption and hydrogenation to CH_4.

Adsorption period	Eq.	Hydrogenation period	Eq.
$Na_2O+CO_2 \leftrightarrows Na_2CO_3$	(12)	$Na_2CO_3 \leftrightarrows Na_2O+CO_2$	(16)
$CaO+CO_2 \leftrightarrows CaCO_3$	(13)	$CaCO_3 \leftrightarrows CaO+CO_2$	(17)
$2NaOH+CO_2 \leftrightarrows Na_2CO_3+H_2O$	(14)	$CO_2+4H_2 \leftrightarrows CH_4+2H_2O$	(18)
$Ca(OH)_2+CO_2 \leftrightarrows CaCO_3+H_2O$	(15)	$CaO+H_2O \leftrightarrows Ca(OH)_2$	(19)
		$Na_2O+H_2O \leftrightarrows 2NaOH$	(20)

description of the temporal evolution of reagents and products, as well as the reactions that take place, were included in previous works [17, 18], as well as their modeling and simulation [34,35]. As a general reminder, Table 2 collects the main reactions governing the CO_2 storage and the CO_2 hydrogenation to CH_4 in each period. The reactions describing the interactions between H_2O and the adsorption sites are also detailed.

During the adsorption period, CO_2 is adsorbed to form carbonates. Since DFM is composed of Na and Ca, both carbonates (Eqs. (12) and (13), Table 2) can be formed. On the other hand, CO_2 can also be adsorbed on a hydrated site, releasing a molecule of H_2O (Eqs. (14) and (15), Table 2). During the hydrogenation period, the decomposition of carbonates (Eqs. (16) and (17), Table 2) takes place, the hydrogenation of CO_2 to form CH_4 (Eq. (18), Table 2) and part of the H_2O produced gets adsorbed onto the basic site, forming hydroxides (Eqs. (19) and (20), Table 2).

The amount of CO_2 stored during the adsorption period, as well as the productions of CH_4, CO and H_2O in each period, are shown in Table 3. The amount of CO_2 stored shows a downward trend. In the first cycle, 345 μmol g^{-1} are stored. In the second cycle, the amount stored is notably reduced to 266 μmol g^{-1}, to stabilize in the last cycles (5–7) at 243 μmol g^{-1}. At the beginning of the first cycle, the DFM is completely regenerated after the high temperature and long duration reduction pretreatment (as detailed in the experimental section). Therefore, there are no adsorbed carbonates on the storage sites and the CO_2 adsorption capacity is maximum. After the first adsorption period, the hydrogenation period is not able to completely decompose the stored carbonates, i.e. some carbonates remain adsorbed irreversibly onto the strong basic sites. Consequently, the CO_2 adsorption capacity is somewhat reduced and is stabilized in the subsequent cycles. This fact reveals that under the operating conditions studied, some storage sites are irreversibly occupied by CO_2 and do not participate in the cyclic process of CO_2 adsorption and hydrogenation to CH_4. By contrast, CH_4 production shows an upward trend with the cycle number. In the first cycle, 197 μmol g^{-1} are produced and production quickly stabilizes at approximately 240 μmol g^{-1}.

Regarding H_2O production, it is detected in both periods (adsorption and hydrogenation), as shown in Fig. 1. During the hydrogenation period, H_2O is formed through the CO_2 hydrogenation (Eq. (18), Table 2) and part of the H_2O produced remains adsorbed, forming hydroxides (Eqs. (19) and (20), Table 2). In the following CO_2 adsorption period, water is displaced by CO_2 from the adsorption sites and is released to the gas phase (Eqs. (14) and (15), Table 2). On the other hand, a small amount of CO is also produced in both periods. In the hydrogenation period, only 1 μmol g^{-1} is produced due to the high H_2/CO_2 ratio [36], which shifts the selectivity towards CH_4. In fact, the selectivity to CH_4 is higher than 99.5% in the seven cycles (42 min of time-on-stream). In the adsorption period, CO is produced by the partial hydrogenation of CO_2 with small amounts of H_2, which remain chemisorbed in the metallic sites from the previous hydrogenation period. Exceptionally, no CO is produced in the adsorption period of cycle 1. This observation is assigned to the fact that the hydrogen chemisorbed in the metallic sites during the hydrogenation pretreatment is released during the stabilization at 340 °C in Ar prior to beginning the cycles.

Table 3 also collects the error with which the carbon balance (s_{CB}) is closed and the H_2O/CH_4 ratio. The s_{CB} is calculated from Eq. (6). The first cycle presents an error of − 42.6%, which confirms that part of the CO_2 is irreversibly adsorbed; that is to say, some CO_2 is adsorbed but not released and hydrogenated to CH_4 or CO. Then the error decreases with the cycle number. In fact, the error is less than 2% for cycles 4–7. On the other hand, the H_2O/CH_4 ratio shows a downward trend that stabilizes at values close to 2 for the last cycles (Table 3). Note that the stoichiometric H_2O/CH_4 ratio of the Sabatier's reaction (Eq. (18), Table 2) is 2. It

Table 3
Stored CO_2 and CH_4, H_2O and CO and productions during the adsorption and hydrogenation periods for the first seven cycles performed with a 1.5% of CO_2 during the adsorption period. The error with the carbon balance are closed (s_{CB}) and the ratio H_2O/CH_4 are collected.

Cycle	Period	CO_2 storage[a]	Y_{CH4}[a]	Y_{H2O}[a]	Y_{CO}[a]	s_{CB}, %	Ratio H_2O/CH_4
1	Adsorption	345	–	67	0	-42.6	2.21
	Hydrogenation	–	197	370	1		
2	Adsorption	266	–	124	3	-11.7	2.09
	Hydrogenation	–	231	363	1		
3	Adsorption	257	–	124	3	-5.8	2.05
	Hydrogenation	–	238	369	1		
4	Adsorption	248	–	120	3	-1.6	2.03
	Hydrogenation	–	240	370	1		
5	Adsorption	243	–	121	3	0.4	2.04
	Hydrogenation	–	240	373	1		
6	Adsorption	242	–	121	3	0.4	2.04
	Hydrogenation	–	239	371	1		
7	Adsorption	243	–	120	3	0.8	2.02
	Hydrogenation	–	241	372	1		

[a] in μmol g^{-1}.

is suggested that values greater than 2 for the first cycles are due to the release of adsorbed H_2O during the hydrogenation pretreatment.

3.2. Influence of the CO_2 concentration on the global performance of the DFM

Fig. 2 shows the evolution of CH_4 and CO productions for cycles 3–22 (Fig. S1a) in which the CO_2 concentration varies in the range 1.5–15% during the adsorption period. In general, as the CO_2 concentration increases, the production of CH_4 and CO increases. This increase is especially pronounced for CH_4 production when the CO_2 concentration increases from 1.5% to 5%. In fact, 240 μmol g^{-1} of CH_4 are produced with 1.5% CO_2, while 305 μmol g^{-1} with 5% CO_2, which represents an increase of 27%. It is proposed that a higher concentration of CO_2 facilitates the diffusion through the carbonate layer to reach the nucleus of the adsorbent and continue forming carbonates. Gruene et al. [37] in their study of CaO/Al_2O_3 adsorbents claim that two distinct kinetic regimes are observed for CO_2 adsorption, a very rapid uptake followed by a slower adsorption, which is probably limited by CO_2 diffusion through the newly formed calcium carbonate crust. With a further increase of the CO_2 concentration from 5% to 10% and from 10% to 15%, the production of CH_4 also increases but to a lesser extent, up to 320 μmol g^{-1} (5% increase) and 328 μmol g^{-1} (2% increase), respectively. The CO_2 concentration in the flue gases is usually in the range 5–15%. Therefore, it is proposed that the CO_2 concentration is not a critical parameter to take into account and that the DFM studied can produce remarkable amounts of CH_4 for a wide range of CO_2 concentrations. Furthermore, the selectivity to CH_4 remains above 99.5% in all cycles. On the other hand, the concentration of CO_2 would influence the duration of the adsorption period. In our previous work [35], the cyclic process was simulated and optimized. It was observed that the percentage of adsorbed CO_2 decreased with increasing adsorption time and for a given CO_2 concentration, the adsorption time coinciding with bed saturation was selected as optimal. Therefore, depending on the CO_2 concentration, the duration of the adsorption period should be selected. However, as seen above, in the range of typical concentrations of the exhaust gases, the CO_2 concentration does not influence the production of CH_4.

3.3. Influence of the concentration of O_2 on the global performance of the DFM

The main advantage of the integrated CO_2 capture and utilization technology (ICCU) with respect to the conventional CO_2 capture and utilization technology (CCU) is the elimination of the costly CO_2 purification step. For this, the direct adsorption of CO_2 is carried out from the flue gases of a combustion process in which oxygen could also be present [38]. Therefore, the influence of the presence of O_2 during the CO_2 adsorption period is analyzed. First, the effect of the incorporation of 10% O_2 together with 1.5% CO_2 is studied. The presence of a low concentration of CO_2 allows higher resolution and higher accuracy for the determination of the amount of CO_2 stored through Eq. (4). Fig. 3 shows the evolution of the amount of CO_2 stored, the CH_4 and CO productions and the amount of CO_2 released during the hydrogenation period for the cycles with 1.5% CO_2 (25−29) and the cycles with 1.5% CO_2 and 10% O_2 (30−34). In the last cycle including CO_2 alone during the adsorption period, i.e. cycle 29, 240 μmol g^{-1} of CH_4 are produced, whereas 195 μmol g^{-1} are produced with the incorporation of O_2 in cycle 30. This initial decrease is followed by a progressive deactivation that reduces the production of methane to 177 μmol g^{-1} for cycle 34. Clearly, the CH_4 production is diminished by the presence of 10% of O_2. Zheng et al. [32] also observed the loss of activity due to the presence of O_2 during the process of adsorption of CO_2 and hydrogenation to CH_4 in successive cycles. These authors justified the decrease in activity due to the oxidation of the active phase during the adsorption period.

The inclusion of oxygen during the CO_2 adsorption period also produces a slight decrease in the amount of CO_2 stored. Note that the amount stored in cycle 29 (CO_2 alone) and in cycle 30 (CO_2 with O_2), represented by hollow circles, is only slightly reduced from 239 to 225 μmol g^{-1} of CO_2. Although the amount of CO_2 stored is hardly affected by the presence of oxygen, the production of methane drops in a higher extent, from 240 μmol g^{-1} of CH_4 to 195 μmol g^{-1} as already detailed. Therefore, the progressive decrease in CH_4 formation (green bars), when CO_2 adsorption is carried out in the presence of O_2, does not seem to be governed by the lower CO_2 adsorption capacity. Instead, it appears that the reduction behavior is limiting the overall performance of the DFM. When some of the Ru species are oxidized to RuO_x due to the presence of oxygen, the reducing ability of DFM is inhibited during the hydrogenation period; consequently, less CH_4 is produced. Furthermore, due to the fact that the adsorption sites are not fully regenerated, the CO_2 adsorption capacity of the subsequent adsorption period is reduced.

In order to have a complete picture of the influence of oxygen on the CO_2 adsorption and hydrogenation to CH_4, additional experiments are carried out in which the concentration of O_2 is varied. In these experiments, the CO_2 concentration is set at 10% to meet industrially relevant conditions and the O_2 concentration is varied in the range 1–10%. Fig. 4 shows the evolution of the production of CH_4 and CO for cycles 50–69 (also included in Fig. S1b) in which the concentration of O_2 is varied. The incorporation of 1% of O_2 reduces the production of CH_4 by 9% (297–273 μmol g^{-1}). With the increase in the O_2 concentration, the production continues to decrease with less pronounced steps down to 250 μmol g^{-1} with the incorporation of 10%.

Unlike CH_4 production, CO production increases when O_2 is introduced during the adsorption period. CO production increases from 2 μmol CO g^{-1} in the absence of O_2 to 3 μmol CO g^{-1} when 10% oxygen

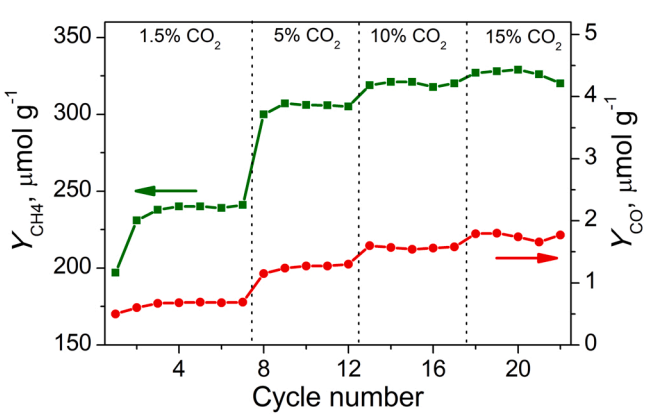

Fig. 2. CH_4 and CO productions for the cycles performed with different CO_2 concentrations during the adsorption period.

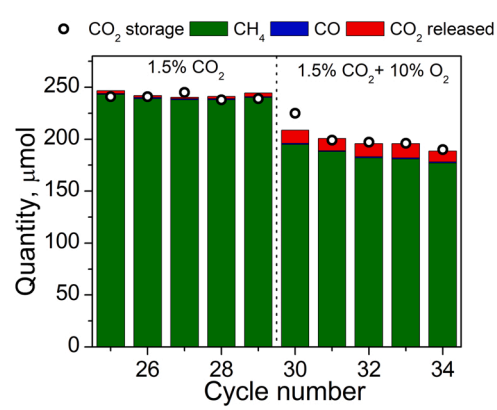

Fig. 3. CH_4 and CO productions and quantities of CO_2 stored (adsorption period) and released (hydrogenation period) during operation with and without 10% oxygen in the adsorption period and a CO_2 concentration of 1.5%.

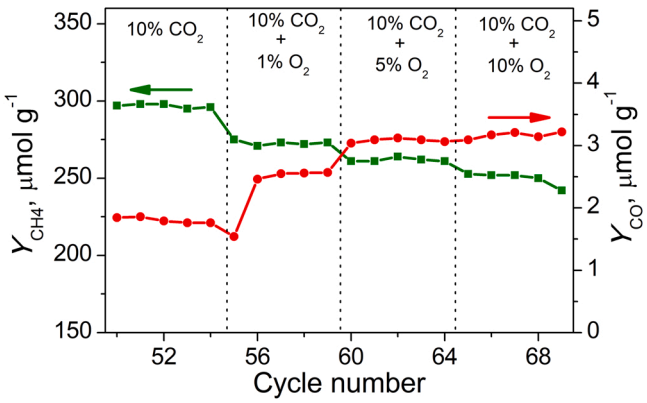

Fig. 4. CH_4 and CO productions for the cycles performed with 10% of CO_2 and different O_2 concentrations during the adsorption period.

is included. It is suggested that the partial oxidation of Ru to RuO_x favors the RWGS reaction and limits the hydrogenation of CO_2 to CH_4. Even though, the amount of CO produced is minimal and a CH_4 selectivity greater than 98.7% is obtained in all cycles.

Fig. 5 shows the evolution of the concentration of reagents and products for representative cycles including 0%, 1%, 5% and 10% O_2 along with 10% CO_2 in the adsorption period. No differences are observed in the CO_2 concentration profiles during the adsorption period (due to the scale of Fig. 5a) regardless of the admitted oxygen concentration. As opposite, some differences are noticed during the hydrogenation period. At the beginning of the hydrogenation period, CO_2 is not detected in the gas phase for the cycle carried out in the absence of oxygen (black curve). This fact indicates that all the CO_2 formed due to the decomposition of carbonates is converted. In contrast, some unreacted CO_2 can be observed for cycles performed in the presence of oxygen during the adsorption period. Furthermore, the concentration of unreacted CO_2 increases as the O_2 concentration increases. The presence of oxygen during the adsorption period oxidizes the metal sites. Therefore, the hydrogenation period begins with the metal sites partially

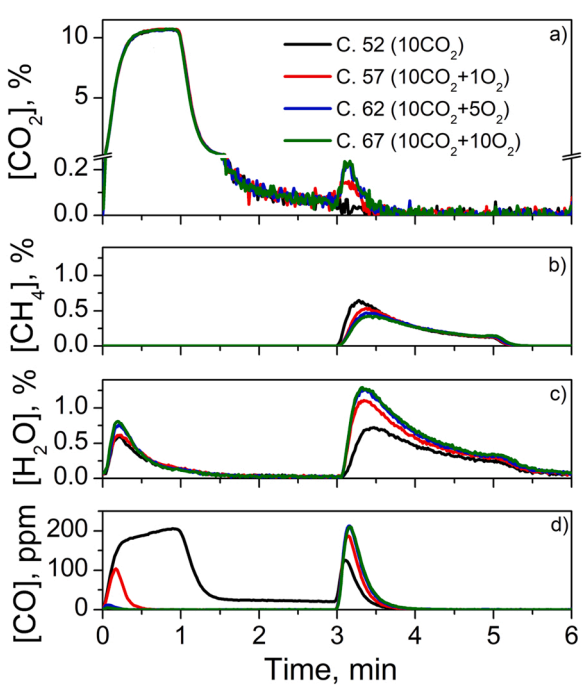

Fig. 5. CO_2, CH_4, H_2O and CO concentration profiles during cycles of CO_2 adsorption and hydrogenation to CH_4 with different O_2 concentrations during the adsorption period.

oxidized. With the incorporation of H_2, the reduction of the oxidized ruthenium sites and the hydrogenation of the desorbed CO_2 occurs simultaneously. However, given the lower availability of active metal sites (reduced, non-oxidized) at the beginning of the hydrogenation period, a small amount of CO_2 leaves the reactor unreacted. As the O_2 concentration increases, a deeper oxidation of the ruthenium sites occurs. This leads to less availability of reduced metal sites where the CO_2 hydrogenation can be catalyzed resulting in a higher concentration of CO_2 leaving the reactor unreacted.

Differences are also observed in the concentration of CH_4 during the hydrogenation period among cycles performed with different O_2 concentration (Fig. 5b). First, it can be observed that the area under the CH_4 curve decreases with O_2 concentration, leading to a lower methane production. Besides, the incorporation of oxygen during the adsorption period also modifies the shape of the evolution of the CH_4 concentration, especially at the beginning of the hydrogenation period. Note that methane formation is progressively delayed as the O_2 concentration increases. This fact can be assigned to the partial oxidation of ruthenium, which consumes hydrogen for its reduction. Once ruthenium is reduced, there is a higher availability of hydrogen, together with a higher fraction of active metal sites, to promote the CO_2 hydrogenation to CH_4. In general, it can be concluded that the production of CH_4 decreases when the adsorption of CO_2 is carried out in the presence of oxygen due to the following facts (ordered by relevance): (i) a lower reduction capacity; (ii) a lower selectivity towards CH_4; (iii) a lower CO_2 adsorption capacity.

The evolution of the H_2O concentration (Fig. 5c) is also affected by the presence of oxygen during the adsorption period. In general, as the O_2 concentration increases, a greater amount of H_2O is produced. A higher oxygen concentration admitted in the adsorption period promotes the oxidation of Ru. Then, during the hydrogenation period, a higher amount of hydrogen is consumed in the reduction of Ru leading to higher concentrations of H_2O. The consumption of additional H_2 in the reduction of oxidized Ru would increase the costs associated with the operation. The amount of H_2 consumed in ruthenium reduction is determined from the amount of H_2O produced and the stoichiometry of the reaction ($RuO_2 + 2\ H_2 \rightarrow Ru + 2\ H_2O$). Specifically, 242 (cycle 57, 1% O_2), 347 (cycle 62, 5% O_2) and 408 μmol g^{-1} (cycle 67, 10% O_2) of H_2 are consumed. However, it is important to note that the duration of the adsorption period is in all cases 1 min. Therefore, during part of the period the DFM is completely saturated, while the metal sites continue to oxidize. At this point, the optimization of the duration of the adsorption period would limit the reduction of the metal sites and therefore the consumption of H_2 in its reduction. This fact would reduce the costs associated with the additional H_2 consumed.

The amount of H_2O released during the adsorption period is also slightly higher. A higher concentration of H_2O during the hydrogenation period favors its adsorption onto the storage sites through Eqs. (19) and (20). Then, CO_2 displaces H_2O from the adsorption sites in the subsequent adsorption period (Eqs. (14) and (15)), releasing a higher amount of H_2O. On the other hand, a higher concentration of O_2 can oxidize the chemisorbed H_2 in the metal sites to a greater extent. This fact also increases the amount of H_2O produced during the adsorption period.

Finally, the evolution of the CO concentration is shown in Fig. 5d. Opposite trends can be observed during the adsorption and hydrogenation periods. While the presence of oxygen during the adsorption period inhibits the formation of CO, its formation is enhanced during the hydrogenation period. For the adsorption period including 1% O_2, the amount of CO produced is significantly reduced with respect to the cycle performed in the absence of oxygen. Furthermore, for cycles performed with 5% and 10% of O_2 CO formation is almost negligible. Previously, we have assigned the formation of CO during the adsorption period to the reaction between chemisorbed H_2, which remains adsorbed onto the metal surface from the previous hydrogenation period, and CO_2 through the RWGS reaction. The inclusion of oxygen during the adsorption period reduces the availability of chemisorbed H_2 (by its oxidation to

H_2O) and consequently CO formation is reduced. On the other hand, CO formation is enhanced during the hydrogenation period with increasing O_2 concentration in the previous adsorption period. The fact that some H_2 is consumed in the reduction of previously oxidized ruthenium sites reduces the H_2 availability (reducing the H_2/CO_2 ratio), which shifts the selectivity towards CO formation in detriment of CH_4.

Finally, cycles are performed alternating adsorption periods including 10% CO_2 in the absence or presence of 10% O_2 in order to study the reversibility of the DFM deactivation due to the presence of O_2, which is evaluated by measuring the production of CH_4. This study is collected in cycles 70–104 in Fig. S1.b of the supporting information. CH_4 production stabilizes at 284 μmol g^{-1} for the O_2-free operation (cycles 70–79, 85–89 and 95–99) and at 244 μmol g^{-1} for the operation including 10% O_2 in the adsorption period (cycles 80–84, 90–94 and 100–104). Note that CH_4 production is totally recovered when oxygen is removed from the flue gas, which reveals that the deactivation of the DFM due to the presence of O_2 is reversible.

3.4. Influence of the concentration of NO_x on the global performance of the DFM

Small amounts of NO_x are usually present in the exhaust gases from combustion processes. Nitrogen in the air, given the high temperatures of the combustion chambers, becomes reactive and reacts with oxygen to give NO_x. Therefore, in this subsection the influence of the presence of NO_x during the adsorption period is studied. Fig. 6 shows the evolution of CH_4 and CO productions for cycles carried out with 10% CO_2 and 0, 400, 800, 1200, 1600 and 2000 ppm of NO (also included in Fig. S1c). In general, the production of CH_4 is slightly reduced as the concentration of NO increases. Fig. S2 shows the evolution of the mean CH_4 production (average of 5 cycles) with the concentration of NO admitted during the adsorption period. A downward linear trend is clearly seen from 271 μmol g^{-1} (0 ppm NO) to 255 μmol g^{-1} (2000 ppm NO). This fact, points out that NO_x and CO_2 compete for the basic adsorption sites. A higher concentration of NO favors its adsorption to the detriment of CO_2 adsorption, which ultimately leads to a lower production of CH_4. Even though, due to the significantly lower concentration of NO with respect to CO_2, CH_4 production is only penalized by around 6% for the operation including 2000 ppm of NO with respect to the absence of NO. On the other hand, CO production is less than 2 μmol g^{-1} irrespective the NO concentration admitted during the adsorption period, which results in a selectivity to CH_4 greater than 99.4%. Based on these results, the suitability of the DFM to operate in the presence of NO_x is demonstrated.

In order to gain insight on the influence of NO_x on the global performance of the DFM, additional experiments were carried out in which the CO_2 concentration was reduced to 1.5% to follow more precisely the evolution of the concentration of reactants and products. In addition, a

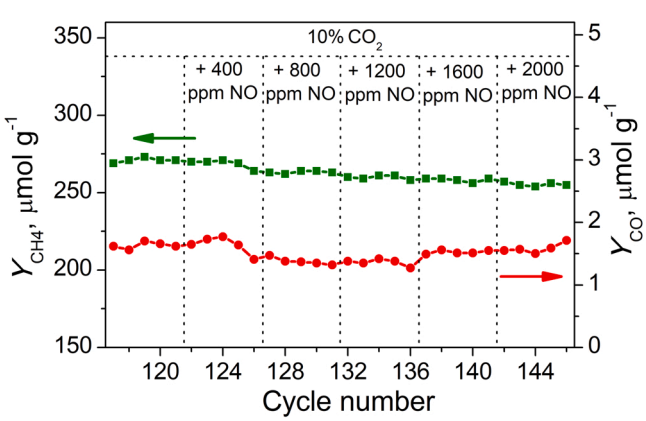

Fig. 6. CH_4 and CO productions for the cycles performed with 10% of CO_2 and different NO concentrations during the adsorption period.

lower concentration of CO_2 was selected to favor the competition between NO and CO_2 for the adsorption sites. Fig. 7 shows the evolution of the concentration of reagents and products in the absence or presence (400 or 2000 ppm) of NO during the adsorption period. CO_2, CH_4, H_2O, CO, NO, NO_2, NH_3 and N_2O were quantified by FTIR whereas nitrogen was qualitatively identified by mass spectrometry following m/e= 28 signal. Additionally, the concentration of CO_2, NO and NO_2 admitted to the reactor are displayed in blue lines. Table 4 shows the distribution of C- and N-based compounds for the cycles shown in Fig. 7, quantified independently for the adsorption and hydrogenation periods, as detailed in the experimental section.

First, we will focus on the evolution of C-based products, i.e. CO_2, CH_4 and CO. The evolution of CO_2 concentration (Fig. 7a) seems almost coincident for the experiments performed in the absence or presence of NO given the scale of the y-axis. However, if the amount of CO_2 stored is calculated by Eq. (4), some differences can be observed. As an example, the amount of CO_2 stored for the experiment carried out in the absence of NO can be calculated by subtracting to the amount of CO_2 fed (743 μmol) the amount of CO_2 (516 μmol), CH_4 (0 μmol) and CO (3 μmol) detected at the reactor outlet during the adsorption period (Table 4), resulting in 224 μmol. Following the same procedure, the amount of CO_2 stored can be calculated for all the experiments, which results in 224, 210 and 203 μmol g^{-1}, for NO concentrations of 0, 400 and 2000 ppm, respectively. Thus, the inclusion of NO limits to some extent the CO_2 storage capacity and reveals a competition between NO and CO_2 for the adsorption sites, as already observed in Fig. S2. CH_4 is only detected during the hydrogenation period (Fig. 7b). In line with the lower CO_2 storage capacity of the DFM in the presence of NO during the adsorption period, lower CH_4 production is observed during the hydrogenation period: 219, 215 and 203 μmol g^{-1} of CH_4 (calculated by Eq. (1)) are produced for cycles carried out with 0, 400 and 2000 ppm of NO, respectively. The evolution of CO during the adsorption and hydrogenation periods is hardly affected by the presence of 400 ppm of NO (Fig. 7d, left). In fact, the same amount of CO (calculated by Eq. (3)) is produced during the adsorption (3 μmol g^{-1}) and hydrogenation (1 μmol g^{-1}) periods in the presence or absence of NO. However, the inclusion of 2000 ppm of NO (Fig. 7d, right) inhibits CO formation during the adsorption period, resulting in the production of 1 μmol g^{-1} of CO. As opposite, CO formation during the hydrogenation period is not affected by the presence of 2000 ppm of NO in the adsorption period.

The evolution of the concentration of N-based species is also included in Fig. 7. NO (accompanied with small amounts of NO_2 in equilibrium) are admitted during the adsorption period (shown in blue in Fig. 7e and f). When 400 ppm of NO is admitted, NO (Fig. 7e, left) and NO_2 (Fig. 7f, left) are not detected at the reactor outlet, revealing that NO_x has been adsorbed on basic sites or converted to other N-based compounds. Oppositely, NO breakthrough is detected around 25 s after the beginning of the adsorption period when 2000 ppm of NO are admitted. This means that the DFM is completely saturated and NO_x leaves the reactor without being stored or converted. Concerning NH_3, similar profiles are recorded in the presence of 400 ppm or 2000 ppm of NO. NH_3 is preferentially detected during the hydrogenation period (Fig. 7g). Taking into account that NO is not admitted during the hydrogenation period (see blue lines in Fig. 7e and f), NH_3 is unequivocally formed upon the hydrogenation of NO_x adsorbed onto the basic sites of the DFM: 11 μmol g^{-1} and 14 μmol g^{-1} of NH_3 are produced (quantified by Eq. (8) in Table 4) when 400 and 2000 ppm of NO are admitted during the adsorption period. On the other hand, small amounts of NH_3 (2 μmol g^{-1}) are detected during the adsorption period. This observation reveals that NO can react with chemisorbed H_2 in the metal sites to produce NH_3, following a similar mechanism as that proposed for the formation of CO. N_2O is not detected in either the adsorption or hydrogenation periods when 400 ppm of NO are admitted (Figure g, left). Small amounts of N_2O are detected during the adsorption period when 2000 ppm of NO are included. The N_2O breakthrough is delayed about 25 s (Fig. 7h, right), as already observed for NO. Thus, N_2O could be

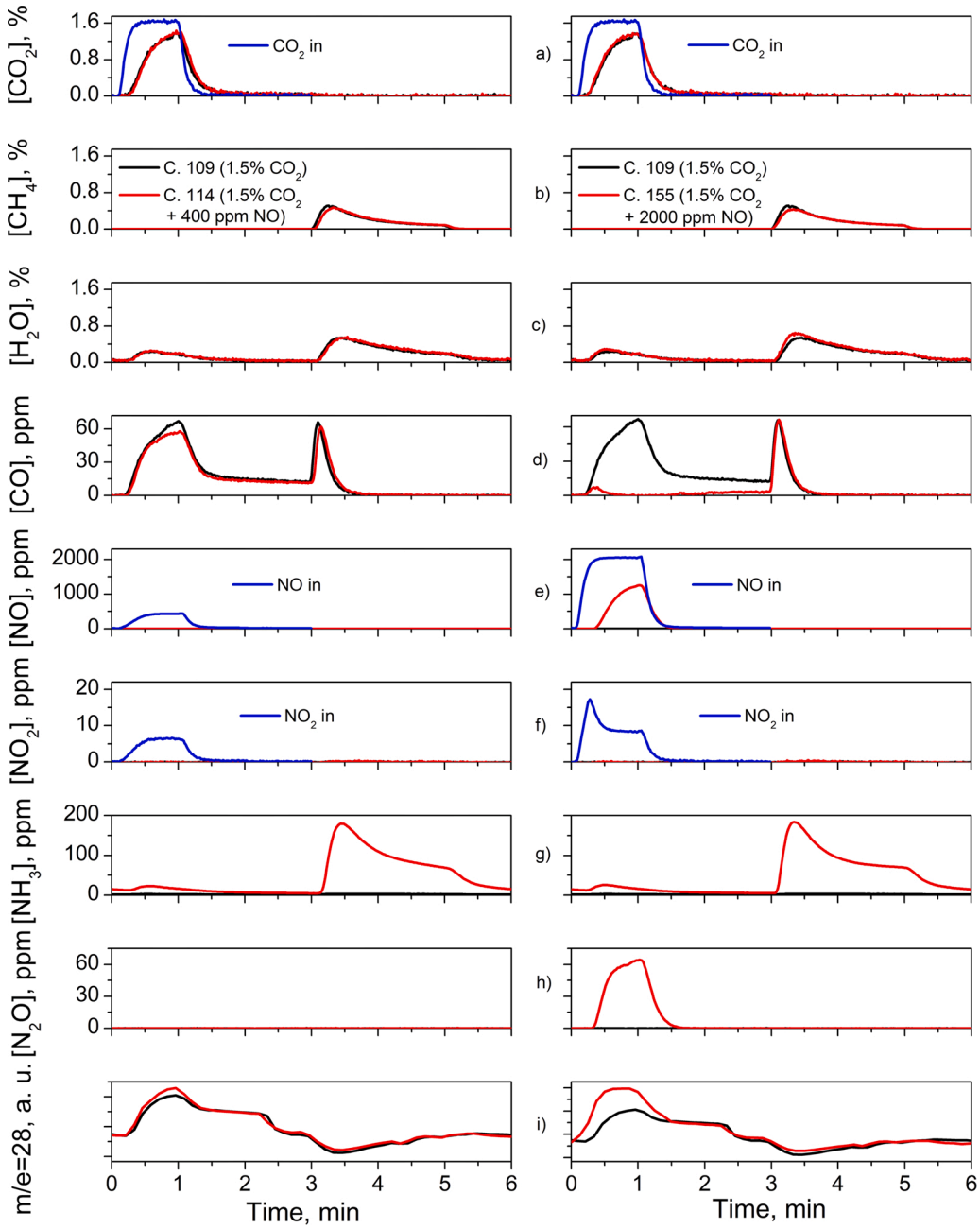

Fig. 7. CO_2, CH_4, H_2O, CO, NO, NO_2, NH_3, N_2O concentration profiles together m/e= 28 signal during cycles of CO_2 adsorption and hydrogenation to CH_4 with different NO concentrations during the adsorption period. The CO_2, NO and NO_2 feed profiles are included in blue.

Table 4
C- and N-compounds distribution of the cycles 109, 114 and 155.

NO, ppm	Amount fed, μmol g^{-1}		Amount stored, μmol g^{-1}		Outlet adsorption period, μmol g^{-1}							Outlet hydrogenation period, μmol g^{-1}						
	CO_2	NO_x	CO_2	NO_x	CO_2	CH_4	CO	NO_x	NH_3	N_2O	N_2	CO_2	CH_4	CO	NO_x	NH_3	N_2O	N_2
0	743	0	224	0	516	0	3	0	0	0	0	0	219	1	0	0	0	0
400	743	19	210	11	530	0	3	0	2	0	3	0	215	1	0	11	0	0
2000	743	101	203	14	539	0	1	39	2	2	21	0	203	1	0	14	0	0

formed due to the reaction between NO and CO, i.e. $2NO+CO \rightarrow N_2O+CO_2$. Note that CO concentration is significantly lower (Fig. 7d, right) for the operation including NO. This observation is in line with the proposed reaction between NO and CO, which reduces the concentration of CO observed at the reactor outlet. The amount of N_2O detected during the adsorption period is 2 μmol g^{-1} (quantified by Eq. (9) in Table 4).

Finally, Fig. 7i shows the evolution of the m/e= 28 signal. As can be observed, the m/e= 28 signal is higher during the adsorption period in the presence of 400 ppm of NO compared to the signal recorded in the absence of NO. This difference is significantly higher when running the adsorption period in the presence of 2000 ppm of NO. This higher m/

e= 28 signal can be attributed to the presence of N_2. Nitrogen can be formed by the reaction between NO and CO ($NO+CO \rightarrow 1/2\ N_2 + CO_2$). The formation of nitrogen by NO reduction with chemisorbed hydrogen cannot be ruled out ($NO+H_2 \rightarrow 1/2\ N_2 + H_2O$).

Nitrogen balance can be applied in the whole operation, including adsorption and hydrogenation periods, to quantify the amount of N_2 formed by Eq. (10). In a cycle-to-cycle steady operation, the sum of N moles in N-containing species at the reactor inlet should match those observed at the outlet. Thus, for the operation with 400 ppm of NO, N_2 moles can be calculated by subtracting to the amount fed (19 μmol g^{-1}) the amount of N moles in N-containing species at the reactor outlet during the adsorption (2 μmol g^{-1} of NH_3) and hydrogenation (11 μmol g^{-1} of NH_3). This results in 6 μmol g^{-1} of N or 3 μmol g^{-1} of N_2. Besides, given the fact that N_2 signal has been only observed during the adsorption period (Fig. 7i), those moles are assigned to be formed during the adsorption period (Table 4). The amount of N_2 produced is increased up to 21 μmol g^{-1} of N_2 when 2000 ppm of NO are admitted during the adsorption period, in line with the significantly higher m/e= 28 signal detected in the right column of Fig. 7i. Once the amount of N_2 is calculated, the amount of NO_x stored on the DFM can be also deduced by Eq. (11): 11 and 14 μmol g^{-1} of NO_x are stored when 400 and 2000 ppm of NO are admitted, respectively. As could be expected, the amount of NO_x stored is increased by a higher concentration of NO, in detriment of CO_2 adsorption. Finally, note that the production of NH_3, N_2O and N_2 causes the consumption of additional H_2. The optimization of the duration of the adsorption period would limit the amount of NO_x stored and, consequently, the production of NH_3, N_2O and N_2. This fact will decrease the amount of H_2 consumed in NO_x reduction.

3.5. Influence of the joint presence of O_2 and NO_x on the global performance of the DFM

In previous sections, the influence of the inclusion of O_2 and NO_x has been studied one by one. In this subsection, the joint effect of O_2 and NO_x in the performance of the DFM is analyzed (Fig. S1d). Fig. 8 shows the evolution of the production of CH_4 and CO in the absence of O_2 and NO (10% CO_2, cycles 162–166), in the presence of NO (10% CO_2 + 400 ppm NO, cycles 167–171) and in the presence of NO and O_2 (10% CO_2 + 400 ppm NO + 10% O_2, cycles 172–176). Then, the procedure is again repeated twice admitting to the reactor the previously defined feed streams in the same sequence. The incorporation of 400 ppm of NO hardly modifies the productions of CH_4 and CO. However, the joint addition of NO and O_2 decreases the production of CH_4 from 269 to 226 μmol g^{-1}, i.e. it is reduced by 19%. The CO production is slightly enhanced by the joint addition of NO and O_2. Even tough, the DFM continues to be highly selective, with a CH_4 selectivity higher than 98.7%.

In the following sequences alternating feed streams with 10% CO_2, 10% CO_2 + 400 ppm NO and 10% CO_2 + 400 ppm NO + 10% O_2, similar evolutions are observed for CH_4 and CO productions. Therefore, no significant loss of activity is detected with the number of cycles. Additionally, the influence of hydrogenating the DFM for 28 min is studied. To do this, in cycle 191 (marked with a empty circle) the duration of the hydrogenation period is extended to 30 min. The amount of methane produced increases from 216 μmol g^{-1} (cycle 190) to 245 μmol g^{-1} (cycle 191). However, in subsequent cycles no significant improvement in CH_4 production is detected.

In order to deepen into the influence of the joint effect of O_2 and NO_x in the performance of the DFM, additional experiments were carried out in which the CO_2 concentration was reduced to 1.5% to accurately follow the evolution of the concentration of reactants and products. Fig. 9 shows the evolution of the concentration of reagents and products with 1.5% CO_2, 10% O_2 and 400 or 2000 ppm of NO during the adsorption period. Additionally, the concentration of CO_2, NO and NO_2 admitted to the reactor are displayed in blue lines. Table 5 shows the distribution of C- and N-based compounds for the cycles shown in Fig. 9, quantified independently for the adsorption and hydrogenation periods.

The joint presence of O_2 and NO increases the CO_2 concentration at the reactor outlet during the adsorption period with respect to the operation in the absence of NO. The previous statement can be more clearly observed for the operation with high NO concentration, i.e. 2000 ppm (Fig. 9a, right). The amount of CO_2 stored results in 229, 209 and 164 μmol when 0, 400 and 2000 ppm of NO along with O_2 are admitted during the adsorption period, respectively (Table 5). The influence of the presence of NO in the CO_2 storage capacity is higher in the presence of oxygen. In fact, when 2000 ppm of NO is admitted during the adsorption period, 203 μmol of CO_2 are stored in the absence of oxygen (Table 4) whereas 164 μmol of CO_2 in the presence of O_2 (Table 5). Thus, the competitive adsorption between NO and CO_2 is enhanced by the presence of oxygen. The lower adsorption capacity of CO_2 results in a lower production of CH_4 during the hydrogenation period (Fig. 9b). Small differences are observed in CO formation by the joint presence of NO and O_2 (Fig. 9d).

The evolution of the concentration of N-based species is also included in Fig. 9 in the presence of O_2 and in the joint presence of O_2 and NO. As can be observed in Fig. 9e, almost no NO is detected at the reactor outlet during the adsorption period, even with the inclusion of 2000 ppm of NO (Fig. 9e, right), which reveals a high adsorption capacity of the DFM. Low concentration of NO_2 (<20 ppm, Fig. 9f) is detected at the reactor outlet when 2000 ppm of NO is admitted. Note that NO_2 concentration at the reactor outlet is higher than that admitted, due to the oxidation of NO to NO_2 in the presence of oxygen. Almost negligible amounts of NH_3, N_2O and N_2 are observed during the adsorption period (Fig. 7g, h and i), as opposite to that observed in the absence of oxygen (Fig. 7). The presence of oxygen consumes all the hydrogen chemisorbed on the metallic sites and impedes the reduction reactions. Overall, the presence of oxygen promotes the adsorption of NO_x to the detriment of CO_2. The amount of NO_x stored result in 18 and 91 μmol when 400 and 2000 ppm of NO is fed along with O_2 during the adsorption period (Table 5). Those amounts are significantly higher than that observed in the absence of O_2 in Table 4. This observation is in line with the NO_x adsorption mechanism reported by Elizundia et al. [39] who concluded that the presence of oxygen enhances NO_x adsorption via formation of nitrates onto basic storage sites. It is proposed that NO is first oxidized to NO_2 (Eq. (21)). Following is the disproportionation reaction (Eqs. (22) and (23)) which has been widely reported on NSR

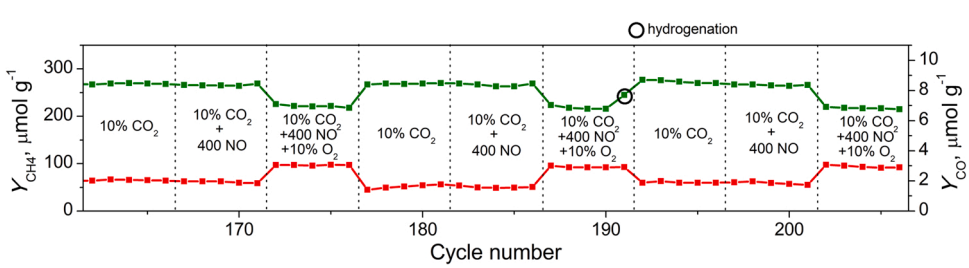

Fig. 8. CH_4 and CO productions in 3 blocks of 15 cycles, in which, every 5 cycles, 10% CO_2, 10% CO_2 + 400 ppm NO or 10% CO_2 + 400 ppm NO + 10% O_2 are fed. The hydrogenation period of the cycle 191 (marked with a circle) is 30 min.

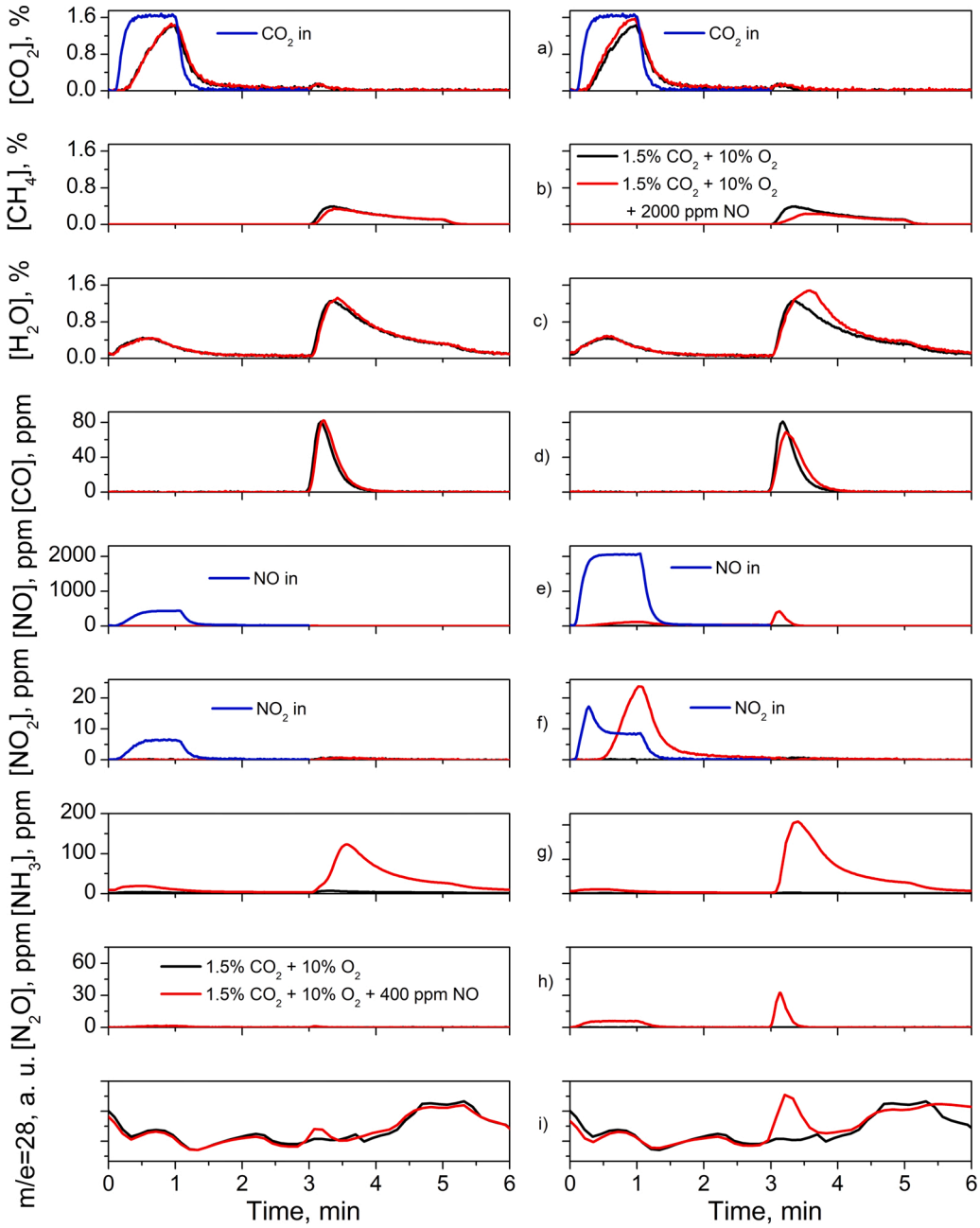

Fig. 9. CO_2, CH_4, H_2O, CO, NO, NO_2, NH_3, N_2O concentration profiles together m/e= 28 signal during cycles of CO_2 adsorption and hydrogenation to CH_4 with 1.5% CO_2, 10% O_2 and 0, 400 or 200 ppm NO during the adsorption period. The CO_2, NO and NO_2 feed profiles are included in blue.

Table 5
C- and N-compounds distribution of the cycles with 1.5% CO_2, 10% O_2 and 0, 400 or 200 ppm NO.

NO, ppm	Amount fed, μmol g^{-1}		Amount stored, μmol g^{-1}		Outlet adsorption period, μmol g^{-1}							Outlet hydrogenation period, μmol g^{-1}						
	CO_2	NO_x	CO_2	NO_x	CO_2	CH_4	CO	NO_x	NH_3	N_2O	N_2	CO_2	CH_4	CO	NO_x	NH_3	N_2O	N_2
0	743	0	229	0	514	0	0	0	0	0	0	9	214	1	0	0	0	0
400	743	19	209	18	534	0	0	0	1	0	0	12	196	1	0	6	0	6
2000	743	101	164	91	579	0	0	8	2	0	0	16	148	1	4	27	1	29

catalysts [40].

$$NO+0.5O_2 \leftrightarrows NO_2 \quad (21)$$

$$Na_2O+3NO_2 \leftrightarrows 2NaNO_3+NO \quad (22)$$

$$CaO+3NO_2 \leftrightarrows Ca(NO_3)_2+NO \quad (23)$$

In the presence of oxygen during the adsorption period, the reduction of NO_x adsorbed species takes place preferentially during the hydrogenation period. Significant amounts of NH_3 and N_2 are detected along with minor amounts of N_2O (Table 5). Those amounts are higher when 2000 ppm of NO is admitted to the reactor, in line with the higher NO_x adsorption capacity.

Porta et al. [30] studied the cyclic operation with O_2, NO_x and steam in the DFM $BaO/Ru/Al_2O_3$. In the adsorption period they fed a stream with 1% CO_2, 2.5% H_2O, 3% O_2 and 500 ppms NO. With the H_2 addition in the hydrogenation period, no C-compounds were detected. The authors assigned this result to the low CO_2 adsorption capacity due to the competitive adsorption between CO_2 and NO_x. However, based on the results of this work, we can conclude that the DFM with the formulation 4%Ru-8%Na_2CO_3-8%CaO/Al_2O_3 is suitable for working in the presence of NO and O_2, presenting still a high production of CH_4.

Finally, the global stability of the material is analysed. With the DFM 4%Ru-8%Na_2CO_3-8%CaO/Al_2O_3, 207 cycles have been carried out on four different days. In total, the DFM has been in operation for 34 h with three stops and intermediate starts. The complete analysis of the global stability is collected in the supporting information. The specific surface area (S_{BET}) is hardly reduced after the operation (131 vs. 128 $m^2\ g^{-1}$) and the XRD spectra (Fig. S5) did not change significantly. However, the metallic dispersion (D_m), determined by H_2 chemisorption, is reduced from 24.8% to 15.9% (corroborated by TEM, Fig. S4). This reduction is assigned to the sintering of the ruthenium during the 34 h of operation, and especially by the addition of oxygen during the adsorption period. Based on this analysis, DFM 4%Ru-8%Na_2CO_3-8%CaO/Al_2O_3 is proposed as suitable for long operating times in the dual process of CO_2 adsorption and hydrogenation to CH_4. DFM has a high resistance to the presence of O_2 and NO_x in the adsorption period. Furthermore, after 34 h of operation, the DFM continues to exhibit adequate physicochemical properties for dual operation.

4. Conclusions

The influence of the presence of oxidizing species, such as O_2 and NO_x, on the CO_2 adsorption and hydrogenation performance of a DFM composed by 4%Ru-8%Na_2CO_3-8%CaO/Al_2O_3 has been studied. In the absence of oxidizing species, it is confirmed that once the cycle-to-cycle steady state is reached, the ICCU process is cyclic and repetitive. In addition, the error with which the carbon balance is closed is low (<2%) and the H_2O/CH_4 ratio is very close to 2, in agreement with stoichiometry of the Sabatier's reaction. As the CO_2 concentration increases, the production of CH_4 increases. A higher CO_2 concentration facilitates the diffusion of CO_2 through the carbonate layer for further formation. For the usual concentration range of CO_2 in combustion exhaust gases (5–15%), the DFM is very effective in the production of CH_4 (305–328 μmol g^{-1}).

The presence of O_2 in the adsorption period decreases the CH_4 production, which is accentuated by increasing the oxygen concentration. The decrease in CH_4 production is mainly attributed to the oxidation of the metal sites that leads to a limitation of the reduction behavior of the DFM. The CH_4 production stabilizes at 244 μmol g^{-1} in the presence of 10% O_2, so it is concluded that the DFM 4%Ru-8%Na_2CO_3-8%CaO/Al_2O_3 is suitable for the cyclic CO_2 adsorption in the presence of O_2 and the subsequent hydrogenation to CH_4.

The addition of NO during the adsorption period (in the absence of oxygen) competes with CO_2 for the adsorption sites. Even so, the feasibility of the DFM to operate in the presence of NO_x is demonstrated. High productions of CH_4, i.e. 215 and 203 μmol g^{-1}, are still produced when 400 or 2000 ppm of NO is admitted during the adsorption period, respectively. N-based products, mainly NH_3, is detected during the hydrogenation period due to the reduction of NO_x adsorbed species. Interestingly, N-based products, such as N_2, N_2O and NH_3 in minor amounts, are also detected during the adsorption period. These compounds can be formed by the reaction between NO and hydrogen chemisorbed on the metal sites in the previous hydrogenation period. The reaction between NO and CO can also explain the formation of N_2 and N_2O. In fact, CO formation is inhibited in the presence of high NO concentrations.

The joint presence of O_2 and NO during the adsorption period, further increases the competitive adsorption of NO and CO_2. NO adsorption is enhanced due to the oxidation of NO to NO_2, which favors nitrates formation onto the basic storage sites. Consequently, CO_2 adsorption is penalized. Even though, still considerable amounts of CH_4, i.e. 196 and 148 μmol g^{-1} are detected when 400 or 2000 oppm of NO are included in the presence of oxygen, respectively. N-based products are detected almost exclusively during the hydrogenation period, as opposite to that observed in the absence of O_2. The reduction of NO_x adsorbed species leads to the formation of N_2 and NH_3 in comparable amounts.

The 207 cycles carried out correspond to 34 h of operation, meanwhile a slight sintering of metallic particles reduces the dispersion of ruthenium. Even so, the DFM has a high resistance to deactivation in the presence of O_2 and NO_x during the adsorption period. Furthermore, after 34 h of operation, the DFM continues exhibiting adequate physicochemical properties for dual operation. Therefore, it can be concluded that DFM 4%Ru-8%Na_2CO_3-8%CaO/Al_2O_3 has a high stability for operation in the presence of O_2 and NO_x.

CRediT authorship contribution statement

Alejandro Bermejo-López: Validation, Methodology, Investigation, Writing – original draft. **Beñat Pereda-Ayo:** Conceptualization, Methodology, Visualization, Writing – review & editing. **Jon A. Onrubia-Calvo:** Methodology, Visualization, Writing – review & editing. **José A. González-Marcos:** Methodology, Data curation, Supervision, Funding acquisition. **Juan R. González-Velasco:** Conceptualization, Supervision, Project administration, Funding acquisition.

Declaration of Competing Interest

The authors declare that they have no known competing financial interests or personal relationships that could have appeared to influence the work reported in this paper.

Data availability

Data will be made available on request.

Acknowledgments

The financial support from the Science and Innovation Spanish Ministry (PID2019-105960RB-C21) and the Basque Government (IT1509-22) is acknowledged. The authors thank for technical and human support provided by SGIker (UPV/EHU Advanced Research Facilities/ ERDF, EU).

Appendix A. Supplementary material

Supplementary data associated with this article can be found in the online version at doi:10.1016/j.jcou.2022.102343.

References

[1] L. Merkouri, T.R. Reina, M.S. Duyar, Closing the carbon cycle with dual function materials, Energy Fuels 35 (2021) 19859–19880.
[2] M. Khezri, A. Heshmati, M. Khodaei, Environmental implications of economic complexity and its role in determining how renewable energies affect CO_2 emissions, Appl. Energy 306 (2022), 117948.
[3] B. Shao, Y. Zhang, Z. Sun, J. Li, Z. Gao, Z. Xie, J. Hu, H. Liu, CO_2 capture and in-situ conversion: recent progresses and perspectives, Green Chem. Eng. 3 (2021) 189–198.
[4] H. Al Baroudi, A. Awoyomi, K. Patchigolla, K. Jonnalagadda, E.J. Anthony, A review of large-scale CO_2 shipping and marine emissions management for carbon capture, utilisation and storage, Appl. Energy 287 (2021), 116510.
[5] M. Dean, J. Blackford, D. Connelly, R. Hines, Insights and guidance for offshore CO_2 storage monitoring based on the QICS, ETI MMV, and STEMM-CCS projects, Int. J. Greenh. Gas Control. 100 (2020), 103120.
[6] I. Ghiat, T. Al-Ansari, A review of carbon capture and utilisation as a CO_2 abatement opportunity within the EWF nexus, J. CO_2 Util. 45 (2021), 101432.

[7] S. Yadav, S.S. Mondal, A review on the progress and prospects of oxy-fuel carbon capture and sequestration (CCS) technology, Fuel 308 (2022), 122057.

[8] E. le Saché, L. Pastor-Pérez, B.J. Haycock, J.J. Villora-Picó, A. Sepúlveda-Escribano, T.R. Reina, Switchable catalysts for chemical CO_2 recycling: a step forward in the methanation and reverse water–gas shift reactions, ACS Sustain. Chem. Eng. 8 (2020) 4614–4622.

[9] M.A. Sabri, S. Al Jitan, D. Bahamon, L.F. Vega, G. Palmisano, Current and future perspectives on catalytic-based integrated carbon capture and utilization, Sci. Total Environ. 790 (2021), 148081.

[10] F. Marocco Stuardi, F. MacPherson, J. Leclaire, Integrated CO_2 capture and utilization: a priority research direction, Curr. Opin. Green Sustain. Chem. 16 (2019) 71–76.

[11] P. Melo Bravo, D.P. Debecker, Combining CO_2 capture and catalytic conversion to methane, Waste Dispos. Sustain. Energy 1 (2019) 53–65.

[12] I.S. Omodolor, H.O. Otor, J.A. Andonegui, B.J. Allen, A. Alba-Rubio, Dual-function materials for CO_2 capture and conversion: a review, Ind. Eng. Chem. Res. 59 (2020) 17612–17631.

[13] S. Sun, H. Sun, P.T. Williams, C. Wu, Recent advances in integrated CO_2 capture and utilization: a review, Sustain. Energy Fuels 5 (2021) 4546–4559.

[14] A.I. Tsiotsias, N.D. Charisiou, I.V. Yentekakis, M.A. Goula, The role of alkali and alkaline earth metals in the CO_2 methanation reaction and the combined capture and methanation of CO_2, Catalysis 10 (2020) 812.

[15] M.S. Duyar, M.A.A. Treviño, R.J. Farrauto, Dual function materials for CO_2 capture and conversion using renewable H_2, Appl. Catal. B Environ. 168–169 (2015) 370–376.

[16] M.A. Arellano-Treviño, Z. He, M.C. Libby, R.J. Farrauto, Catalysts and adsorbents for CO_2 capture and conversion with dual function materials: limitations of Ni-containing DFMs for flue gas applications, J. CO_2 Util. 31 (2019) 143–151.

[17] A. Bermejo-López, B. Pereda-Ayo, J.A. González-Marcos, J.R. González-Velasco, Mechanism of the CO_2 storage and in situ hydrogenation to CH_4. Temperature and adsorbent loading effects over Ru-CaO/Al_2O_3 and Ru-Na_2CO_3/Al_2O_3 catalysts, Appl. Catal. B Environ. 256 (2019), 117845.

[18] A. Bermejo-López, B. Pereda-Ayo, J.A. González-Marcos, J.R. González-Velasco, Ni loading effects on dual function materials for capture and in-situ conversion of CO_2 to CH_4 using CaO or Na_2CO_3, J. CO_2 Util. 34 (2019) 576–587.

[19] A. Bermejo-López, B. Pereda-Ayo, J.A. González-Marcos, J.R. González-Velasco, Alternate cycles of CO_2 storage and in situ hydrogenation to CH_4 on Ni-Na_2CO_3/Al_2O_3: influence of promoter addition and calcination temperature, Sustain. Energy Fuels 5 (2021) 1194–1210.

[20] S. Cimino, F. Boccia, L. Lisi, Effect of alkali promoters (Li, Na, K) on the performance of Ru/Al_2O_3 catalysts for CO_2 capture and hydrogenation to methane, J. CO_2 Util. 37 (2020) 195–203.

[21] S. Cimino, R. Russo, L. Lisi, Insights into the cyclic CO_2 capture and catalytic methanation over highly performing Li-Ru/Al_2O_3 dual function materials, Chem. Eng. J. 428 (2022), 131275.

[22] M.S. Duyar, S. Wang, M.A. Arellano-Treviño, R.J. Farrauto, CO_2 utilization with a novel dual function material (DFM) for capture and catalytic conversion to synthetic natural gas: an update, J. CO_2 Util. 15 (2016) 65–71.

[23] F. Kosaka, Y. Liu, S. Chen, T. Mochizuki, H. Takagi, A. Urakawa, K. Kuramoto, Enhanced activity of integrated CO_2 capture and reduction to CH_4 under pressurized conditions toward atmospheric CO_2 utilization, ACS Sustain. Chem. Eng. 9 (2021) 3452–3463.

[24] A. Porta, R. Matarrese, C.G. Visconti, L. Castoldi, L. Lietti, Storage material effects on the performance of Ru-based CO_2 capture and methanation dual functioning materials, Ind. Eng. Chem. Res. 60 (2021) 6706–6718.

[25] Z. Zhou, N. Sun, B. Wang, Z. Han, S. Cao, D. Hu, T. Zhu, Q. Shen, W. Wei, 2D-layered Ni–MgO–Al_2O_3 nanosheets for integrated capture and methanation of CO_2, ChemSusChem 13 (2020) 360–368.

[26] A. Bermejo-López, B. Pereda-Ayo, J.A. Onrubia-Calvo, J.A. González-Marcos, J. R. González-Velasco, Tuning basicity of dual function materials widens operation temperature window for efficient CO_2 adsorption and hydrogenation to CH_4, J. CO_2 Util. 58 (2022), 101922.

[27] S. Wang, R.J. Farrauto, S. Karp, J.H. Jeon, E.T. Schrunk, Parametric, cyclic aging and characterization studies for CO_2 capture from flue gas and catalytic conversion to synthetic natural gas using a dual functional material (DFM), J. CO_2 Util. 27 (2018) 390–397.

[28] C. Jeong-Potter, R. Farrauto, Feasibility study of combining direct air capture of CO_2 and methanation at isothermal conditions with dual function materials, Appl. Catal. B Environ. 282 (2021), 119416.

[29] M.A. Arellano-Treviño, N. Kanani, C.W. Jeong-Potter, R.J. Farrauto, Bimetallic catalysts for CO_2 capture and hydrogenation at simulated flue gas conditions, Chem. Eng. J. 375 (2019), 121953.

[30] A. Porta, C.G. Visconti, L. Castoldi, R. Matarrese, C. Jeong-Potter, R. Farrauto, L. Lietti, Ru-Ba synergistic effect in dual functioning materials for cyclic CO_2 capture and methanation, Appl. Catal. B Environ. 283 (2021), 119654.

[31] S. Wang, E.T. Schrunk, H. Mahajan, R.J. Farrauto, The role of ruthenium in CO_2 capture and catalytic conversion to fuel by dual function materials (DFM), Catalysts 7 (2017).

[32] Q. Zheng, R. Farrauto, A. Chau Nguyen, Adsorption and methanation of flue gas CO_2 with dual functional catalytic materials: a parametric study, Ind. Eng. Chem. Res. 55 (2016) 6768–6776.

[33] J. Okal, M. Zawadzki, L. Kępiński, L. Krajczyk, W. Tylus, The use of hydrogen chemisorption for the determination of Ru dispersion in Ru/γ-alumina catalysts, Appl. Catal. A Gen. 319 (2007) 202–209.

[34] A. Bermejo-López, B. Pereda-Ayo, J.A. González-Marcos, J.R. González-Velasco, Modeling the CO_2 capture and in situ conversion to CH_4 on dual function Ru-Na_2CO_3/Al_2O_3 catalyst, J. CO_2 Util. 42 (2020), 101351.

[35] A. Bermejo-López, B. Pereda-Ayo, J.A. González-Marcos, J.R. González-Velasco, Simulation-based optimization of cycle timing for CO_2 capture and hydrogenation with dual function catalyst, Catal. Today 394–396 (2021) 314–324.

[36] L. Falbo, M. Martinelli, C.G. Visconti, L. Lietti, C. Bassano, P. Deiana, Kinetics of CO_2 methanation on a Ru-based catalyst at process conditions relevant for Power-to-Gas applications, Appl. Catal. B Environ. 225 (2018) 354–363.

[37] P. Gruene, A.G. Belova, T.M. Yegulalp, R.J. Farrauto, M.J. Castaldi, Dispersed calcium oxide as a reversible and efficient CO_2−sorbent at intermediate temperatures, Ind. Eng. Chem. Res. 50 (2011) 4042–4049.

[38] N. Masiran, D.N. Vo, M.A. Salam, B. Abdullah, Improvement on coke formation of CaO-Ni/Al_2O_3 catalysts in ethylene production via dehydration of ethanol, Procedia Eng. 148 (2016) 1289–1294.

[39] U. Elizundia, R. López-Fonseca, I. Landa, M.A. Gutiérrez-Ortiz, J.R. González-Velasco, FT-IR study of NO_x storage mechanism over Pt/BaO/Al_2O_3 catalysts. Effect of the Pt–BaO interaction, Top. Catal. 42 (2007) 37–41.

[40] S. Andonova, V. Marchionni, M. Borelli, R. Nedyalkova, L. Lietti, L. Olsson, Mechanistic investigations of the promoting role of Rh on the NSR performance of NO_x storage BaO-based catalysts, Appl. Catal. B Environ. 132–133 (2013) 266–281.